Dual Nature of the Electronic Structure of $(La_{2-x-y}Nd_ySr_x)CuO_4$ and $La_{1.85}Sr_{0.15}CuO_4$

X. J. Zhou,[1,2] T. Yoshida,[3] S. A. Kellar,[1] P. V. Bogdanov,[1] E. D. Lu,[2] A. Lanzara,[1,2] M. Nakamura,[2] T. Noda,[4]
T. Kakeshita,[4] H. Eisaki,[4] S. Uchida,[4] A. Fujimori,[3] Z. Hussain,[2] and Z.-X. Shen[1]

[1]*Department of Physics, Applied Physics and Stanford Synchrotron Radiation Laboratory, Stanford University,
Stanford, California 94305*
[2]*Advanced Light Source, Lawrence Berkeley National Lab, Berkeley, California 94720*
[3]*Department of Physics, University of Tokyo, Bunkyo-ku, Tokyo 113, Japan*
[4]*Department of Superconductivity, University of Tokyo, Bunkyo-ku, Tokyo 113, Japan*
(Received 31 August 2000)

High resolution angle-resolved photoemission measurements have been carried out on $(La_{1.4-x}Nd_{0.6}Sr_x)CuO_4$, a model system with static one-dimensional (1D) charge ordering (stripe), and $(La_{1.85}Sr_{0.15})CuO_4$, a high temperature superconductor ($T_c = 40$ K) with possible dynamic stripes. In addition to the straight segments near $(\pi, 0)$ and $(0, \pi)$ antinodal regions, we have identified the existence of spectral weight along the $[1,1]$ nodal direction in the electronic structure of both systems. This observation of nodal state, together with the straight segments near antinodal regions, reveals the dual nature of the electronic structure of stripes due to the competition of order and disorder.

The existence and origin of charge ordering in cuprates and its implication to high temperature superconductivity are at the heart of a great debate in physics [1]. Static one-dimensional (1D) charge ordering (stripe) along the $[1,0]$ or $[0,1]$ direction was first observed in the $(La_{2-x-y}Nd_ySr_x)CuO_4$ (Nd-LSCO) system from neutron scattering [2], with complimentary evidence from other techniques [3–6]. Similar signatures identified in $(La_{2-x}Sr_x)CuO_4$ (LSCO) [7–10] and other high temperature superconductors [11,12] point to the possible existence of stripes in these systems, albeit of a dynamic nature. A key issue about this new electronic state of matter concerns whether the stripe phase is intrinsically metallic or insulating, given its spin and charge-ordered nature, and more significantly, whether it is responsible for high temperature superconductivity [13,14]. Understanding the electronic structure of the stripe phase is a prerequisite for addressing these issues and angle-resolved photoemission spectroscopy (ARPES) proves to be a powerful tool to provide this essential information [15]. In this paper, we report detailed ARPES results on the electronic structure of $(La_{1.4-x}Nd_{0.6}Sr_x)CuO_4$ with static stripes and a related superconductor $La_{1.85}Sr_{0.15}CuO_4$ ($T_c = 40$ K) with possible dynamic stripes. With high resolution ARPES spectra densely collected under various measurement geometries, we have identified in both systems the existence of spectral weight along the $[1,1]$ nodal direction, where the superconducting gap is zero in d-wave pairing symmetry. The observation of nodal spectral weight, which is not compatible with ideal stripes along the $[1,0]$ or $[0,1]$ direction, combined with the straight segments near $(\pi, 0)$ and $(0, \pi)$ antinodal regions expected from 1D stripes [6], provides a complete view of the dual nature of the electronic structure of the stripe phase, revealing the competition of order and disorder in these systems.

The experiment was carried out at beam line 10.0.1.1 of the Advanced Light Source [6]. The angular mode of the Scienta analyzer (SES-200) allows one to measure an angle of $\sim 14°$ simultaneously, corresponding to $\sim 1.1\pi$ in the momentum space for the 55 eV photon energy we used (the unit of momentum is defined as $1/a$ with a being the lattice constant). The momentum resolution is 0.02π and the energy resolution is 16–20 meV. To check for polarization dependence and the matrix element effect [16], we used various measurement geometries. (1) The sample was preoriented so that the analyzer scan is along the crystal axis a (Cu-O bonding direction). The mapping was realized by rotating the sample to change the polar angle (Fig. 1). (2) The sample is oriented so that the analyzer scan spans the diagonal direction. The mapping is realized by *rotating the analyzer* to change the polar angle while keeping the sample fixed (Fig. 2). In the first configuration, the electrical field vector $\vec{E}$ of the incident light is nearly normal to the sample surface, while for the second configuration, it is parallel to the sample surface. The k-space sampling is highly dense; the maps reported here are constructed from nearly 10 000 energy distribution curves (EDCs). The $(La_{1.4-x}Nd_{0.6}Sr_x)CuO_4$ ($x = 0.10$ and 0.15) and $(La_{2-x}Sr_x)CuO_4$ ($x = 0.15$, $T_c = 40$ K) single crystals were grown using the traveling floating zone method which were characterized by various techniques [2,3,5]. The sample was cleaved *in situ* in vacuum and measured at 15 K with a base pressure of $(2–5) \times 10^{-11}$ Torr.

Figure 1 shows the spectral weight of the Nd-LSCO ($x = 0.10$ and 0.15) samples. The data for the $x = 0.12$ sample, taken under the same experimental condition, were previously reported [6]. The integration windows are set at 30 and 300 meV from the Fermi level, which approximately represent the Fermi level feature $A(k, E_F)$ and the momentum distribution function $n(k)$, respectively, modi-
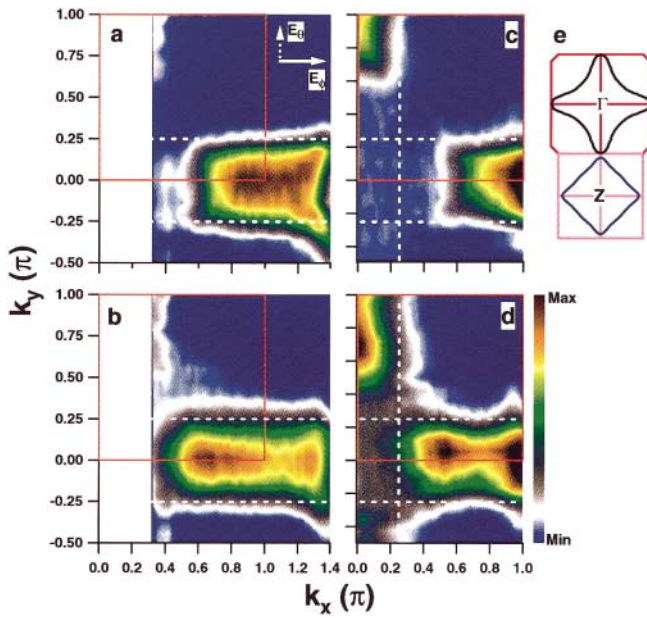
FIG. 1 (color). Spectral weight of Nd-LSCO with different doping levels, x, integrated within different energy windows near the Fermi level. (a) $x = 0.10$, 30 meV; (b) $x = 0.10$, 300 meV; (c) $x = 0.15$, 30 meV; (d) $x = 0.15$, 300 meV. The boundary of the spectral weight can be approximated as $|k_x| = \pi/4$ and $|k_y| = \pi/4$ lines (dashed white lines). In the inset in (a) is the in-plane electrical field component. For comparison, the LDA calculated Fermi surface is included in (e) where the top part shows the Fermi surface at $k_z = 0$ (black line) and the lower part the Fermi surface at $k_z = \pi/c$ (blue line) [18].
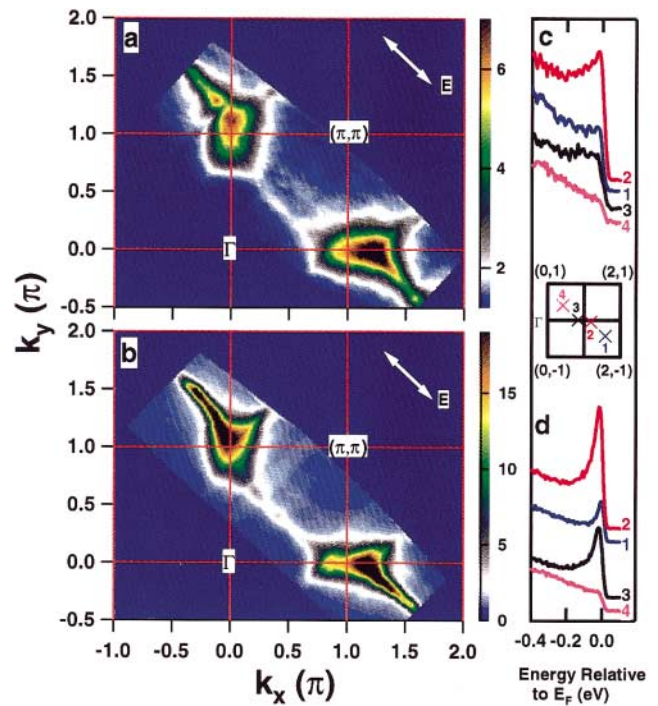

FIG. 2 (color). Spectral weight of Nd-LSCO ($x = 0.15$) (a) and LSCO ($x = 0.15$) (b) integrated within a 30 meV energy window near the Fermi level. Typical EDC spectra near the nodal and the $(\pi, 0)$ regions, as indicated in the in-between inset, are shown in (c) and (d) for Nd-LSCO and LSCO, respectively. The in-plane electrical field is also indicated which was fixed during the measurement.

fied by the photoionization matrix element [17]. The low energy spectral weight for both samples [Figs. 1(a) and 1(c)] is confined near the $(\pi, 0)$ and $(0, \pi)$ regions. Upon increasing the energy integration window, the spectral weight extends to the center of the Brillouin zone (Γ point) [Figs. 1(b) and 1(d)]. In both cases, the spectral weight is confined within the boundaries defined by $|k_x| = \pi/4$ and $|k_y| = \pi/4$ (white dashed lines in Fig. 1). It is noted that, while the boundary of the spectral weight confinement for the $x = 0.10$ sample is very straight, it shows a small wavy character for the $x = 0.15$ sample [Fig. 1(d)], which is related to another intensity maximum clearly discernible near $k_x = 0.5\pi$. Similar results have also been observed for the $x = 0.12$ sample [6] and this wavy effect appears to get stronger with doping.

The data in Fig. 1 are difficult to reconcile with the band structure calculations where the local-density approximation (LDA) calculated Fermi surface runs more or less diagonally ($[1, -1]$ direction) [see Fig. 1(e)] [18]. We have done a matrix element simulation for this measurement geometry and found that the spectral weight near the $(\pi/2, \pi/2)$ nodal region is suppressed compared with the $(\pi, 0)$ and $(0, \pi)$ antinodal regions [19]. Nevertheless, it is still impossible to reproduce the observed spectral weight confinement with straight boundaries parallel to the $[1, 0]$ or $[0, 1]$ direction, even by considering matrix element effects as well as the k_z effect. On the other hand, a simple

stripe picture seems to capture the main characteristics of the data in Fig. 1 if one considers the low energy signal as mainly being from metallic stripes [6,20–23]. The momentum distribution function $n(k)$ [Figs. 1(b) and 1(d)] then suggests two sets of Fermi surfaces, defined by the $|k_x| = \pi/4$ and $|k_y| = \pi/4$ lines, which can be understood as a superposition of two 1D Fermi surfaces originating from two perpendicularly oriented stripe domains. The $\pi/4$ boundary lines are related to the fact that the stripes are approximately quarter-filled in the charge stripes [2,6]. The possible superposition of two orthogonal 1D Fermi surfaces in LSCO has also been proposed theoretically from the perspective of the t-J model [24].

However, the above rigid stripe model also leaves many questions unanswered. A prominent one relates to the fast dispersion seen along $(0, 0)$ to $(\pi, 0)$ direction within the 200 meV of the Fermi level, which implies a charge motion perpendicular to vertical stripes [6]. The concomitant carrier motion along stripes and transverse to stripes points to the possible existence of a nodal state along the $[1, 1]$ diagonal direction.

To gain more insight into the issue of nodal state, we focused our measurements on the nodal regions by covering along the diagonal direction (Fig. 2). We also extended the measurement to the second zone considering a possible different matrix element for different zones. To enhance

the signal from the nodal region, the in-plane electric field is maximized by fixing the $\vec{E}$ vector parallel to the sample surface. Our matrix element simulations show spectral weight enhancement in the nodal region for this measurement geometry [19]. Figure 2 shows the low energy excitations for both Nd-LSCO ($x = 0.15$) and La$_{1.85}$Sr$_{0.15}$CuO$_4$ samples, measured under such a condition. One sees the similar straight segments near $(0, \pi)$ and $(\pi, 0)$ as seen in Fig. 1 even though the *a-b* planes of the samples were rotated 45° with respect to each other. More importantly, it is possible to see the spectral weight near the $(\pi/2, \pi/2)$ nodal region for both samples, although the signal in the first zone is weaker than that in the second zone. This shows that, while the spectral weight is suppressed along the nodal direction [6,25], it is nevertheless present and detectable under favorable conditions. The EDC spectra near the nodal regions show a well-defined Fermi cutoff [Figs. 2(c) and 2(d)], indicating the metallic nature of these systems.

As seen from Figs. 1 and 2, there are two aspects involved in the electronic structure of the stripe phase. The first is the straight segment near the $(\pi, 0)$ and $(0, \pi)$ antinodal regions. The feature is very robust as it is seen under different measurement geometries, which appears to be a measure of the ordered nature of stripes. The second feature is the nodal state seen in Fig. 2, which is sensitive to doping and measurement geometry. This feature is likely a measure of deviation from the ideal stripe case, which may be due to disorder or dynamic fluctuations. We note here that we have observed two similar features in Nd-LSCO with $x = 0.10$ and in LSCO with a doping level as low as $x = 0.07$ [26]. The nodal signal appears to get stronger with increasing Sr doping for both Nd-LSCO and LSCO, and for a given Sr doping level, it is stronger in LSCO than in Nd-LSCO samples [26]. As seen from Figs. 2(a) and 2(b), near the $(\pi, 0)$ region in the second zone, the maximum intensity contour extends all the way from the nodal region and intersects with the $(\pi, 0)$-$(2\pi, 0)$ line, suggesting an electronlike Fermi surface. Interestingly, this Fermi surface is reminiscent of that from the LDA calculation [Fig. 1(e)] [18].

A complete description of the electronic structure of the stripe phase needs to take both of the above two aspects into account: the straight segment near the antinodal region and the spectral weight near the nodal region with its associated Fermi surface. Figure 3 highlights these two features in the first Brillouin zone for the Nd-LSCO ($x = 0.15$) and LSCO ($x = 0.15$) samples, which are also schematically depicted in Fig. 3(c) (upper-left panel). While it seems to be straightforward to associate the straight segments with stripes because of their 1D nature [20], the detection of spectral weight near the nodal region in the *static* stripe phase poses a new challenge to our understanding of this charge-ordered state because the nodal spectral weight is expected to be suppressed in a simple stripe picture [21,22]. The experimental
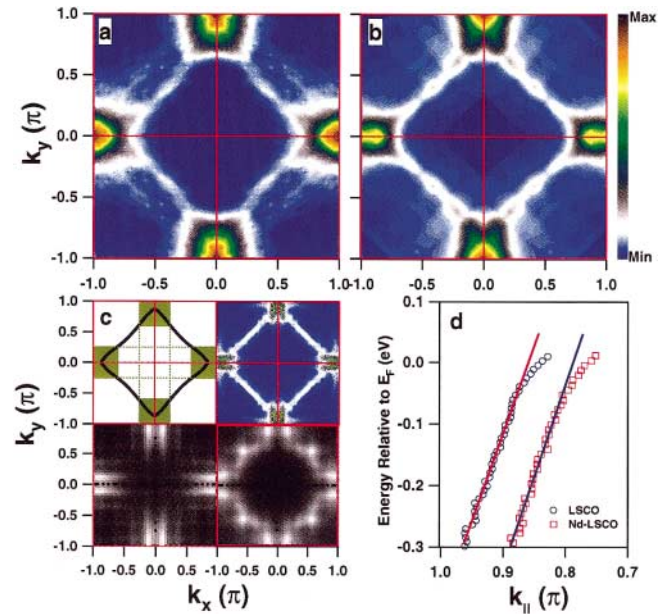

FIG. 3 (color). Measured low energy (30 meV integration) spectral weight of Nd-LSCO ($x = 0.15$) (a) and LSCO ($x = 0.15$) (b), as obtained by symmetrizing the first zone data of Fig. 2. The observed two features are schematically illustrated in (c) (upper-left panel): diamond-shaped nodal Fermi surface (black line) and 1D spectral confinements near $(\pi, 0)$ and $(0, \pi)$ regions. The spectral weight patterns calculated from stripe fluctuation (upper-right panel) [20], from the site-centered stripe (lower-left panel) and bond-centered stripe (lower-right panel) [28] are also included in (c) for comparison. The matrix element effect, which is clearly present in the data, is not incorporated in the calculations. (d) shows the dispersion along the nodal direction (in the second zone) for the Nd-LSCO and LSCO samples; a slope breakdown in the dispersion can be seen for both cases at nearly −50 meV. The dispersion is obtained by fitting momentum distribution curves which show a well-defined Lorentzian line shape. The dispersion for Nd-LSCO is horizontally offset for clarity, with the two solid lines as a guide to the eye.

question regarding the origin is whether they originate from another distinct phase or they are intrinsic properties of the same stripe phase. In the case of phase separation, this would mean that, besides stripes, there is another nonstripe metallic phase with a much higher carrier concentration, as estimated from the Luttinger volume of the diamond-shaped Fermi surface (Fig. 3). As far as we know, there is little evidence of such a phase separation in Nd-LSCO and LSCO systems at the doping level discussed here [25], although it has been observed in a related La$_2$CuO$_{4+\delta}$ system [11].

The detection of nodal spectral intensity in the stripe system provides a clear distinction of the stripe physics from the ordinary 1D charge motion in a rigid 1D system. In the stripe context, the nodal Fermi surface may arise from disorder or fluctuation of stripes where the holes leak into the antiferromagnetic region [20,23]. Here disorder also induces the effect that the antiferromagnetic region may not be fully gapped when it becomes very narrow.

The measured spectral weight in Fig. 3 for Nd-LSCO and LSCO is similar to the one calculated based on such a disordered stripe picture [Fig. 3(c), upper-right panel] [20]. This also seems to be consistent with the trend that in LSCO the nodal spectral weight is more intense than that in Nd-LSCO because the stripes in the former are dynamic while they are static in the latter. However, the dispersion of the two systems [Fig. 3(d)] is very similar. Note that, in this picture, the nodal Fermi surface is actually a superposition of Fermi surface features from two perpendicular stripe domains; for an individual stripe domain, this Fermi surface feature can be discrete [20,23].

An alternative scenario to understand the two features in the stripe context is a possible coexistence of site- and bond-centered stripes [27]. Both types of stripes are compatible with neutron experiments [2] and are close in energy as indicated by various calculations [28]. As shown in Fig. 3(c), a combination of the calculated $A(k, E_F)$ patterns for the site-centered (lower-left panel) and bond-centered stripes (lower-right panel) [27] can reproduce the data. While the site-centered stripe shows little spectral weight near the nodal region [21,22,27], the bond-centered stripe is compatible with the nodal state [27]. It is therefore tempting to associate the 1D straight segment to site-centered stripes and the nodal Fermi surface feature to bond-centered stripes. Since these two types of stripes are different in their wave functions, it may also help explain why they show different behaviors under different measurement conditions. If this picture proves to be true, it would imply that, with increasing doping, bond-centered stripes are produced at the expense of site-centered stripes, and more bond-centered stripes may be generated as the stripes become more dynamic (Fig. 3). This seems to further suggest that the bond-centered stripes are more favorable for superconductivity than the site-centered stripes; a possibility remains to be investigated further. We note that the above scenarios can be closely related to each other. Stripe disorder or fluctuation may naturally give rise to hole-rich and hole-poor regions as in the phase separation case, particularly with the possible existence of stripe dislocations in the system. In the case of stripe fluctuation, the randomness in the stripe separations may necessarily give rise to a mixture of site-centered and bond-centered stripes.

[1] For a review, see V. J. Emery, S. A. Kivelson, and J. M. Tranquada, cond-mat/9907228; J. Zaanen, J. Phys. Chem. Solids **59**, 1769 (1998), and references therein.
[2] J. M. Tranquada *et al.,* Nature (London) **375**, 561 (1995); J. M. Tranquada *et al.,* Phys. Rev. B **59**, 14 712 (1999).
[3] M. v. Zimmermann *et al.,* Europhys. Lett. **41**, 629 (1998).
[4] A. W. Hunt *et al.,* Phys. Rev. Lett. **82**, 4300 (1999).
[5] T. Noda, H. Eisaki, and S. Uchida, Science **286**, 265 (1999).
[6] X. J. Zhou *et al.,* Science **286**, 268 (1999).
[7] S. W. Cheong *et al.,* Phys. Rev. Lett. **67**, 1791 (1991).
[8] T. E. Mason *et al.,* Phys. Rev. Lett. **68**, 1414 (1992).
[9] A. Bianconi *et al.,* Phys. Rev. Lett. **76**, 3412 (1996).
[10] K. Yamada *et al.,* Phys. Rev. B **57**, 6165 (1998).
[11] B. O. Wells *et al.,* Science **277**, 1067 (1997); Y. S. Lee *et al.,* Phys. Rev. B **60**, 3643 (1999).
[12] H. A. Mook *et al.,* Nature (London) **395**, 580–582 (1998).
[13] V. J. Emery *et al.,* Phys. Rev. B **56**, 6120 (1997).
[14] S. A. Kivelson *et al.,* Nature (London) **393**, 550 (1998).
[15] Z.-X. Shen and D. S. Dessau, Phys. Rep. **253**, 1 (1995).
[16] A. Bansil and M. Lindroos, Phys. Rev. Lett. **83**, 5154 (1999).
[17] Th. Straub *et al.,* Phys. Rev. B **55**, 13 473 (1997).
[18] J.-H. Xu *et al.,* Phys. Lett. A **120**, 489 (1987); W. E. Pickett, Rev. Mod. Phys. **61**, 433 (1989).
[19] T. Yoshida *et al.,* Phys. Rev. B **63**, 220501 (2001).
[20] M. I. Salkola, V. J. Emery, and S. A. Kivelson, Phys. Rev. Lett. **77**, 155 (1996).
[21] T. Tohyama *et al.,* Phys. Rev. Lett. **82**, 4910 (1999).
[22] M. Fleck *et al.,* Phys. Rev. Lett. **84**, 4962 (2000).
[23] R. S. Markiewicz, cond-mat/9911108.
[24] H. Yamase and H. Kohno, J. Phys. Soc. Jpn. **69**, 332 (2000).
[25] A. Ino *et al.,* J. Phys. Soc. Jpn. **68**, 1496 (1999); cond-mat/9902048; cond-mat/0005370.
[26] T. Yoshida *et al.* (unpublished).
[27] M. G. Zacher *et al.,* Phys. Rev. Lett. **85**, 2585 (2000).
[28] S. R. White and D. J. Scalapino, Phys. Rev. Lett. **80**, 1272 (1998).